Journal of Manufacturing Processes 84 (2022) 230–239

Contents lists available at ScienceDirect

Journal of Manufacturing Processes

journal homepage: www.elsevier.com/locate/manpro

Study on mass concentration and morphology of SMAW fume particles with a new covered electrode using nano-$CaTiO_3$ as an arc stabilizer

M. Rahul [a], S.P. Sivapirakasam [a,*], Sreejith Mohan [a], B.R. Vishnu [b], J.F.P. Gomes [c,d]

[a] Industrial Safety Engineering Lab, Department of Mechanical Engineering, National Institute of Technology, Tiruchirappalli, India
[b] Department of Mechanical Engineering, Marian Engineering College, Kerala, India
[c] CERENA - Centro de Recursos Naturais e Ambiente, Instituto Superior Técnico, Universidade de Lisboa, Av. Rovisco Pais, 1, 1049-001 Lisboa, Portugal
[d] Departamento de Engenharia Química, Instituto Superior de Engenharia de Lisboa, R. Conselheiro Emidio Navarro, 1, 1959-007 Lisboa, Portugal

ARTICLE INFO

Keywords:
Welding fume
Nano-$CaTiO_3$ powder
Particle mass concentration
Mass median aerodynamic diameter
Particle morphology

ABSTRACT

Advances in manufacturing emphasize on the development of sustainable and green manufacturing processes. Welding is a popular manufacturing process practiced worldwide. The paper presented here describes a new covered electrode for a shielded metal arc welding (SMAW) process wherein nano-sized calcium titanate ($CaTiO_3$) powder was used as an arc stabilizer, replacing the conventional micro sized $CaTiO_3$ in the flux. The effect of this flux modification on the mass concentration and morphology of welding fume particulates was systematically investigated. The mass concentration of coarse, fine and sub-micron sized fume particulates was measured by segregating the fumes in a four-stage personal cascade impactor. The particle mass distribution was estimated from the mass median aerodynamic diameter (MMAD) and geometric standard deviation (GSD) of the fume particulates. The morphology of fumes at each impactor stage was analysed using scanning electron microscopy and its count median diameter (CMD) was determined. The results indicated as much as 48 % reduction in total fumes and 54 % reduction in the breathing zone concentration of fumes when the entire $CaTiO_3$ in the electrode flux was substituted with nano-$CaTiO_3$. Morphological analysis indicated that a large fraction of the fumes from the conventional electrode were polydispersed particles, while the new electrodes predominantly contained monodispersed particles which have a relatively faster rate of removal from the lungs. Overall, the present work indicated that introducing nano sized $CaTiO_3$ as an arc stabilizer to the flux covering of SMAW electrode could not only reduce the hazardous fume emissions but also reduce its biological activity and toxicity, thus making the process more sustainable and environment friendly.

1. Introduction

Welding fumes are inherently toxic and continued exposure to them can cause several occupational health disorders ranging from acute effects like metal fume fever, cough and pneumonia to chronic obstructive lung diseases such as bronchitis [1–3]. Fine fume particles smaller than 2.5 μm can easily enter the respiratory system and lodge in the alveolar region of the lungs, causing respiratory disorders [4]. The International Agency for Research on Cancer (IARC) recently reclassified welding fume from Group 2B ('possibly carcinogenic to humans') to Group 1 ('carcinogenic to humans') [5]. The toxicity of welding fumes depends on particle mass concentration, morphology and its size, apart from its composition and reactivity, which varies with the welding process and the consumables used [6].

SMAW is by far the most widely employed process in industries such as steel construction, shipbuilding, petroleum, nuclear, marine, and aerospace [7]. Nevertheless, it produces large quantity of fumes compared to other arc welding processes. Fume generation in SMAW is by and large attributed to the melting and evaporation of the consumable electrode, though the base metal also has a minor contribution [8]. Considering the above facts, leads to a tremendous impetus in research towards achieving reduction of fumes in the SMAW process.

The principle sources of fumes in SMAW are the consumable electrode and base metal. Suitable modification of the consumable electrode proved to reduce fume levels. These modifications were primarily aimed at improving the arc stability by adding materials to the electrode with low ionization potential. Materials such as Al_2O_3, TiO_2 and $CaCO_3$ in their nano-sized form, were found to have immense potential in

* Corresponding author.
E-mail address: spshivam@nitt.edu (S.P. Sivapirakasam).

https://doi.org/10.1016/j.jmapro.2022.10.015
Received 14 June 2022; Received in revised form 29 September 2022; Accepted 5 October 2022

reducing fumes without compromising weld quality. Consumable modification using nano-sized Al_2O_3 and TiO_2 particles to the welding electrode in the form of a coating on the core welding wire prior to the flux coating reduced fume concentration by 60 % and 75 %, respectively [9–10]. In a separate study, fume level and concentration of Cr (VI) were reduced when their nano-sized counterpart replaced the conventional micro-sized $CaCO_3$ in the welding flux [11].

The size, mass, and shape of the fume particle determines the location of the deposit in the respiratory tract. The biological activity of inhalable welding fume particles is determined by their number density, size, shape, and specific surface, as represented by lower moments of particle size distribution (PSD). Various studies have shown that particle size ranged from 0.005 to 20 μm in welding fumes. Particles with an aerodynamic diameter larger than 10 μm were almost fully trapped in the upper respiratory system. Particles of 5–10 μm size lodge in the main and small breathing passages. Fine particles with an aerodynamic diameter 1–2.5 μm settle in bronchi region. Submicron particles with a size of less than 1 μm penetrate deep into the bronchi and alveolar region. Hence it is essential to determine the concentration of coarse, fine and sub-micron particulate matter in welding fumes. Numerous approaches are available in place to determine mass distributions of welding fumes, including cascade impactors, scanning mobility particle sizers, and optical particle counters [12]. Cascade impactors are widely utilised for size classification and the size-classified chemical analysis of aerosols due to their ease of construction, operation, and relatively sharp cut-off characteristics. Other than size concentration, the morphology of fume particulates has, also, received increasing attention due to its effect on their radiative and chemical properties [13–15]. Data on the particle size and the morphology of the welding fume is also important to understand their biological activity and toxicity to human health [16].

The present study describes a novel method for increasing the arc stability in a shielded metal arc welding process by replacing the conventional micro sized $CaTiO_3$ in the flux with nano-$CaTiO_3$ at varying proportions by weight. Nano $CaTiO_3$ was selected due to its potential to improve the arc stability, slag mobility and the bonding characteristics of weld. The effect of adding nano-$CaTiO_3$ on the total fume formation rate and breathing zone concentration of fumes were systematically evaluated. The mass concentration of coarse, fine and submicron sized fume particles were analysed using a four-stage cascade impactor. The morphological analysis of fumes from each impactor stage were carried out using scanning electron microscopy. The paper addresses that the addition of the arc stabilizer not only reduced the hazardous emissions from welding, but also reduced its biological activity and toxicity, hence making the process sustainable, safe and environment friendly.

2. Materials and methods

2.1. Preparation of welding electrodes

SS316 L rod (diameter 4 mm and length 350 mm) was used as the core wire of the electrode. The weld was laid on SS 316L plates (diameter 300 mm and thickness 10 mm) fixed on a rotating plate with variable speed, inside the fume chamber. The elemental composition of the welding core wire is shown in Table 1 and the flux formulation of E316-L16 in Table 2. A schematic of the electrode making procedure and the structure of the electrode is shown in Fig. 1.

The experimental electrodes labelled C1, C2, C3, C4, and C5 were prepared by substituting micro sized calcium titanate in the flux with nano-calcium titanate (Make: NANOSHEL, 98 %, 80 nm particle size) in varying proportions of 20 %, 40 %, 60 %, 80 %, and 100 % respectively. The conventional E316-L16 electrode was labelled as 'N'. Both set of electrodes were produced in the same electrode extrusion setup (Make: Logos, Model: EP 50). The addition of nano $CaTiO_3$ particles had apparently no negative effect on the extrusion behaviour of the electrodes. The flux coating was strong and moisture resistant, with a uniform surface texture comparable to the conventional welding electrode (N).

Table 2
E316-L16 flux chemistry.

Elements	Composition (% by weight)
Rutile	20–50
Titanium oxide	10–15
Sodium silicate	1–5
Ferro silicon	0.1–1
Calcium carbonate	15–18
Chromium	15–25
Nickel	3–9
Calcium titanate	6–9
Molybdenum	0–4
Calcium fluoride	2–10
Cryolite	0–5
Field spar	0–3
Niobium	0–3
Ferro manganese	1–3
Chromium (III) oxide	0–0.5
Potassium silicate	1–5
Potassium hydroxide	0–0.5

2.2. Welding and fume measurement

Fume formation rate (FFR) signifies the concentration of welding fume in a confined workplace with hardly any ventilation. It calculates how much fume a certain consumable or gas emits in a given amount of time under established welding conditions. Bead on plate welding was carried out on circular base plates, inside the fume test chamber, constructed according to the guidelines of the American Welding Society (AWS) ISO 15011-1, 2009 [17]. Fig. 2 illustrates the fume test chamber used for the study.

Prior to welding, the base plates were thoroughly cleaned with a wire brush to clean off dust and rust. A welding power supply with a of constant current type DC rectifier (ARC 400, RILION) was used with the current being set at 140 A. Welding was carried out by a trained welder and performed at a set speed of 15 cm/min, with an average feed rate of 18 cm/min and 15°–30° of electrode pull angle. The resultant fumes were extracted at a flow rate of 900 l/min, and forced to be deposited on a 253 × 204 mm dimension. Whatman GF/A filter paper with a 1.6 μm pore. To increase the efficiency of the collection, the extractor fan was run for 90 s after initial welding for 60 s. Fume formation rate (FFR) was measured from the weight difference of the filter paper as per the following Eq. (1).

$$\text{Fume formation rate} = \frac{F_w - I_w}{t}\ g \Big/ min.... \quad (1)$$

where I_w denotes the initial weight of filter paper, F_w the final weight of filter paper and 't' the time taken for welding. Both fume collection and

Table 1
Base plate and core wire chemical composition.

	Element (wt%)									
	Mn	Mo	Ni	Cr	S	Si	N	P	C	Fe
Base metal	1.5–2	1.8–3.5	9–14	14.5–18.5	0.02	1	0.12	0.045	0.03	Bal.
Core wire	1–2	1.5–5.5	8–13	4.5–19.5	0.03	1.2	0.12	0.050	0.02	Bal.

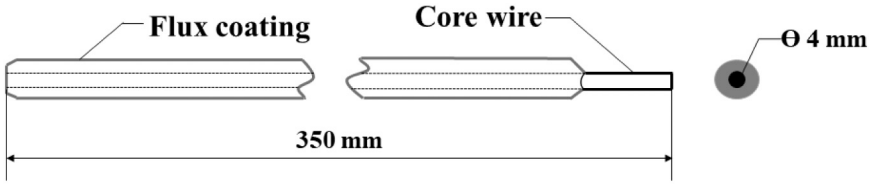

Fig. 1. Schematic diagram of structure of electrode.

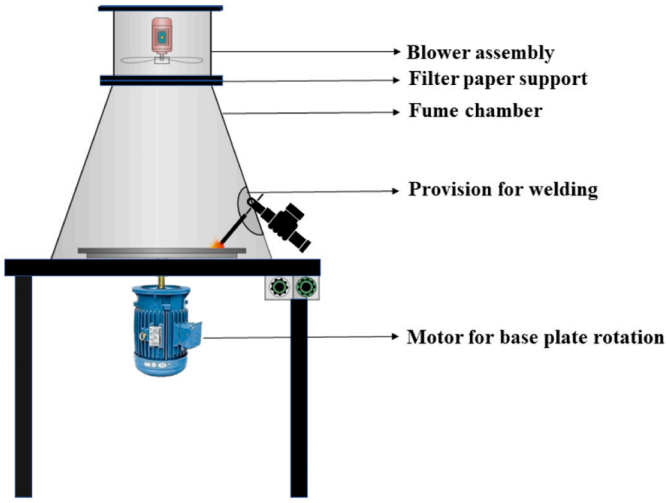

Fig. 2. Schematic diagram of fume test chamber.

measurement were carried out in triplicate for each type of electrode and the average value of FFR was noted.

2.3. Measurement of breathing zone concentration of fumes

Breathing zone samples, on the other hand, were collected from a hazily defined zone surrounding the head to assess worker exposure to airborne contaminants. This zone is theoretical to have an airborne concentration equivalent to the worker's breathing. The sampling of airborne particles in the welder's breathing zone was carried out according to ISO 10882-1 standard procedure [18]. A personal air sampler (Make: SKC, Model: 224-PCXR8) was used for this purpose. Bead-on-plate welds were deposited by a trained welder using the conventional and experimental electrodes at a current of 140 A. The fumes so produced were collected in the breathing zone using a filter paper placed on one of the lapels of the welder. The filter was made of poly vinyl chloride (PVC) and had an average pore size of 1.6 μm. The welder used a face mask with the filter cassette being positioned behind it.

Prior to measurement, a soap bubble meter was used to calibrate the air sampler at a 2 l/min flow rate. Both welding and fume sampling were performed in controlled test room conditions for 12 min. The room dimensions were 120 × 108 in., with a single ventilation of 24 × 12 in.. The sampler flow rate was set at 2 l/min. The air velocity in the room was observed to be was 0.1 m/s, when measured with an anemometer. After sampling, the weight of the filter paper was measured and compared with the weight before sampling to get the breathing zone concentration. The weight difference of the filter paper before and after sampling was used to determine the concentration in the breathing zone as per the following Eq. (2):

$$\text{Breathing zone concentration} = \frac{(W_a - W_b) \times 1000}{fxt}\ \text{mg}\Big/\text{m}^3 \ldots. \quad (2)$$

where W_a and W_b are the weights of the filter paper (mg) after and before sampling, 't' the sampling time (min), and 'f' the sampler flow rate (l/min).

2.4. Spatter measurement

Formation of welding spatter can have a significant effect on fume formation rate. Spatter represents large surface area from which further evaporation occurs and contributes to fume formation. An infrared camera (Make: Flir; Model: SC 7500-MB) was used to capture the spatters emitted during welding with conventional and experimental electrodes. The images were rendered at 350 frames/s and the thermal images were obtained using the infrared imaging software ALTAIR 5.50. All images were captured at 1 m distance from the welding zone having a focal length of 25 mm.

2.5. Segregation of particle size

Emission of particulate matters (PM) from the fume was collected using a four-stage cascade impactor (Model: 100-3002, SKC, Inc.) with 0.5 μm pore and a 25 mm diameter polytetrafluoroethylene (PTFE) filter (Cat. No. 225-3708, SKC, Inc.). Particles of size below 0.25 μm were collected on a 2 μm pore size 37 mm diameter PTFE filter. The sample pump of the impactor was maintained to ensure a flow rate of 9 l/min.

2.5.1. Data analysis

2.5.1.1. Particle mass concentration. The mass concentration of fume particulates collected at various stages in the impactor were determined from the difference of Post-sampling and Pre-sampling weights of the filter paper [19–20]. All samples were taken simultaneously, and the results averaged among three samples.

The mass distribution of the particles was described using the mass median aerodynamic diameter (MMAD) and the geometric standard deviation (GSD) of d_{50}.The MMAD is defined as the diameter for which half the mass is contributed by a particle larger than the MMAD and half by particles smaller than MMAD. If the MMAD is less than 2 μm or is unknown, a high-efficiency particulate air filter (filtering efficiency of 99.97 % or higher) or any filter certified to 42 CFR 84 (95 % or higher filtering efficiency) has to be used, according to the National Institute of Occupational Safety and Health Guidelines [21]. Arc welding operations generate particles with a diameter of less than 2 μm or lower. As a result, the MMAD of welding fume plays an important role in occupational safety.

2.5.1.2. Particle morphology and particle size. Environmental epidemiology studies suggest that the harmful effect of inhaled particles is determined not only by particle mass but also its morphology and size. The morphology of the fume particulates collected at various stages in the cascade impactor were analysed using scanning electron microscope (SEM) (Carl Zeiss, Zeiss) [22–24]. Both spatter particles and heated metal droplets generate large amounts of supersaturated metal vapours, which then nucleate to create solid particles. Condensation and coagulation occur, as these particles cool down to ambient temperatures, resulting in the production of chain aggregates and agglomerates [25]. Particle morphology has to critically considered as it determines the surface area and aerodynamic diameter of a particle. The SEM images were subsequently post processed using the image analysis software

ImageJ, to determine the particle size collected on each impactor plate. At least 200 particles were measured per stage and a count median diameter (CMD) and respective geometric standard deviation (GSD) determined [26–27]. The CMD defines the fraction of total number of particles for any size range.

3. Results and discussion

3.1. Fume formation rate and breathing zone concentration

Fume formation rate (FFR) and the breathing zone concentration (BZC) of fumes from conventional and experimental electrodes were measured and compared as depicted in Fig. 3.

All experimental electrodes (C1 to C5) indicated a lower fume formation rate and breathing zone concentration compared to the conventional electrode (N) clearly indicating the favourable effect of nano-$CaTiO_3$ in the flux. Among the experimental electrodes, the highest reduction of 48.85 % in FFR and 54.04 % in BZC was noticed in the electrode C5, with 100 % nano $CaTiO_3$ in its flux. The following reasons could explain the reduction of fumes.

$CaTiO_3$ among other materials like TiO_2, Al_2O_3, ZrO_2 and $CaCO_3$ exhibit arc stabilizing properties in the flux. $CaTiO_3$ as an arc stabilizer dissociates into CaO and TiO_2 in the arc plasma, as given in the Eq. (3).

$$TiO_2 \rightarrow Ti^{4+} + O_2^{2-} \ldots. \quad (3)$$

These materials have low ionization potential in the sense that they are easily ionized in the arc and act as effective charge carriers enabling adequate arc ignition and reignition characteristics [28]. A more stable arc would imply low fume levels. Moreover, as the spatter density decreases, it would lead to reduced evaporation from its surface which results in a low fume level.

As the size of $CaTiO_3$ reduces to nano scale, there is a concomitant increase in its effective surface area resulting in improved electron emission capacity [29]. This would mean a higher rate of decomposition of $CaTiO_3$ into CaO and TiO_2. Calcium titanate assays 41.03 % CaO and 58.45 % TiO_2. The CaO and TiO_2, decompositions (as shown in Eqs. 4 and 5) promote the presence of charged Ca^{2+} and Ti^{4+} in the arc atmosphere which further improves electron emission capacity leading to, better ionization and arc stability.

$$CaO_3 \rightarrow Ca^{2+} + O^{2} \ldots. \quad (4)$$

$$TiO_2 \rightarrow Ti^{4+} + O_2^{2-} \ldots. \quad (5)$$

As the content of nano $CaTiO_3$ in the flux increases, both arc ionization and arc stability improve. This would explain the reason behind the significant fume reduction in electrode C5 containing 100 % nano $CaTiO_3$.

A more realistic approximation of the stability of the arc could be obtained from the spatter images shown in Fig. 4. The main process causing spatter when welding with rutile electrodes is the CO_2 gas explosion during short circuit breakage. Reducing the ionization potential of the covering of the rutile electrode is of importance when designing a rutile electrode to produce minimum spatter. The white spots encircled with red are the spatters generated during welding. As obvious from Fig. 4, the conventional electrode generated more spatters, compared to the experimental electrode C5 indicating the superior arc stability in C5 due to which fumes were reduced. Enhanced arc stability contributed to improved process stability and spatter reduction. Coarse fume particles are formed by mechanical mean like ejection of spatters from the arc or the molten weld pool. Increase in spatter size and density leads to higher evaporation of metals from the surface and also to higher fume [30]. The size and density of conventional spatter particles is relatively high compared to the experimental electrodes.

3.2. Mass concentration of fume particulates

Fig. 5 shows the mass concentration at each impactor stage for different electrode compositions. A systematic addition reduction in mass concentration with the addition of nano $CaTiO_3$ can be observed from the figure. A reduction of 98.75 % in PM 2.5, 96 % in PM 1, 68.1 % in PM 0.5 and 48.8 % in PM 0.25 were observed with the C5 electrode combination. In conventional welding electrodes 73.16 % of the fume were greater than 2.5 μm while in the experimental electrodes C1, C2, C3, C4, and C5, 20.96 %, 11.48 %, 18.62 %, 10.32 % and 8.13 % PM were higher than 2.5 μm. Hence, a notable reduction in coarse particle formation was observed in the experimental electrode. It was further observed that for all electrodes, the mass concentration of PM in the fine region (1–2.5 μm) was comparatively lower than that in the remaining regions. Hence, it was conclusive that, among the particulates emitted, a considerable amount fell in the coarse region with the remainder going to the lower sub-micron region (0.25–1 μm). The above variations in PM concentration may be explained as follows.

The major contributor to the formation of coarse fume particles (observed at the impaction stage A) was the ejection of micro spatters. Such particles are formed by the ejection and explosion of liquid droplets consisting predominantly of molten welded metal and electrode components [31]. Micro spatter formation in conventional and experimental electrodes could be substantiated from Fig. 4. It is apparent that spatters formed in the nano-$CaTiO_3$ coated electrodes are much lower compared to the conventional electrode. This could be the reason for a lower concentration of coarse fume particles in the experimental electrodes. Yet another observation from the Fig. 5 is that, for all electrodes,

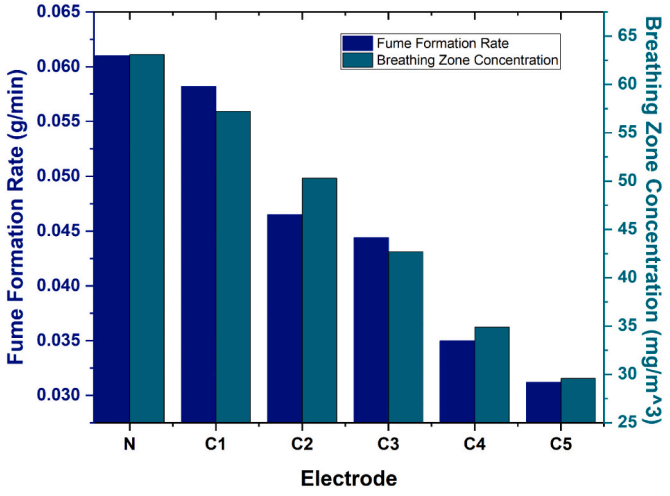

Fig. 3. Fume formation rate and breathing zone concentration from conventional and experimental electrodes.

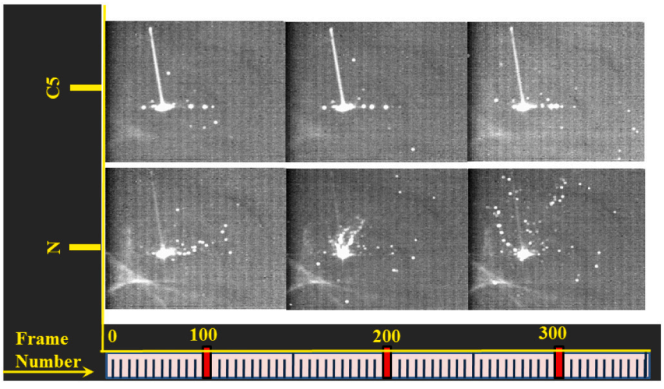

Fig. 4. Infrared camera images of spatter formation at three different frames (100, 200 and 300).

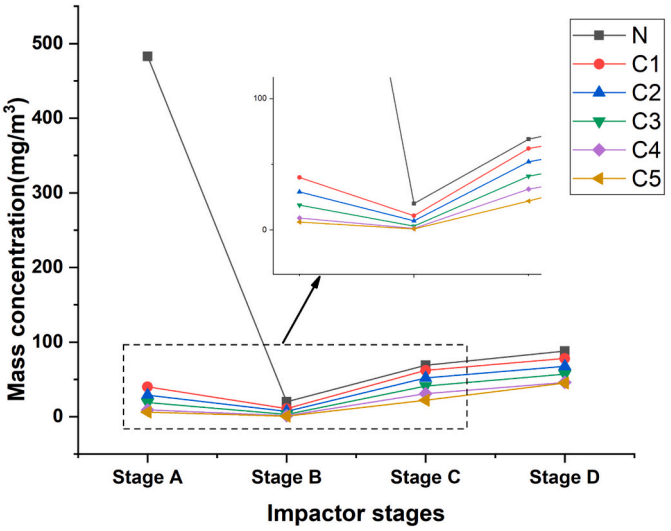

Fig. 5. Mass concentration of conventional and experimental electrodes.

the mass concentration of fume particulates reduced at the second impaction stage. The fume particles generated after welding were charged particles and tended to collide. Impaction stage B is designed to collect fume particulates in a size range of 1–2.5 μm. During the experiment, the impactor was placed at the welder's collar. While travelling from the source to the impactor, most of these generated particles tend to collide with each other and form higher-sized particles. For this reason, most fume particles generated in a particle size range 1–2.5 μm may collide with each other while moving and thereby contribute mass at the initial impactor stage 2.5–10 μm, which reduces the concentration in impactor stage B. The agglomeration effect and mass reduction in fume particles at impactor stage B was evident from the SEM analysis shown in Fig. 8 [12].

Whereas, the higher concentration of sub-micron particles (at impaction stages C and D) for all electrodes might be attributed to the phenomenon of initial welding burst [32]. The evaporation followed by the bursting, resulted in the generation of nano-particles of less than 50 nm size. These nano-particles, in turn, formed chain like agglomerates of an average size of 0.5 μm. These micro-sized agglomerates contributed to the higher mass concentration at the lower impactor stages (stages C and D). As, the experimental electrodes had better arc stability and reduced spatter formation than conventional electrodes, fume mass concentrations at these stages was lower.

Due to the foregoing effects, the mass concentration of coarse and sub-micron fume particles increased at impactor stages A, C and D, while, the concentration of fine fume particles (1–2.5 μm) decreased at impaction stage B.

The influence of nano material addition on fume particle size can be analysed using the mass median aerodynamic diameter. The MMAD was found from the cumulative probability curve of the welding fume particles shown in Fig. 6. It is simply the intersection or extrapolation of data through the 50th percentile. Table.3 shows the mass median aerodynamic diameter (MMAD) and geometrical standard deviation of both conventional and experimental electrodes obtained from Fig. 6. The MMAD value obtained from the conventional electrode was 0.3787 μm which was the highest obtained diameter. MMAD values depend on the rate of fume generation (quantity of fumes). Higher fume generation leads to agglomeration of particles and increases MMAD. The reduction in MMAD was calculated to be, 0.10 % for C1, 0.34 % for C2, 2.3 % for C3, 3.69 % for C4 and 4.96 % for C5. Though reduction of MMAD was not preferable, compared to the 48.85 % reduction in FFR and 54.04 % reduction in BZC, reduction in the MMAD was within 4.96 %, which would not cause any significant effect.

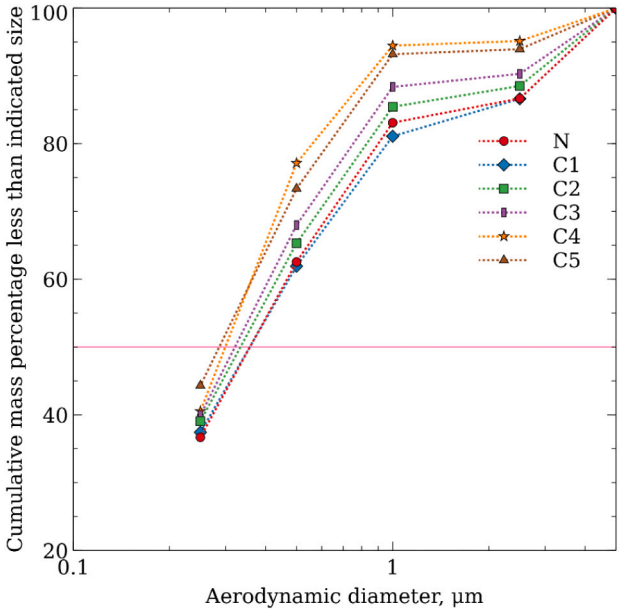

Fig. 6. Lognormal probability plot of welding fume particle captured with cascade impactor.

Table 3
Mass median aerodynamic diameter (MMAD) and geometrical standard deviation (σ_g) of welding fume particles collected with cascade impactor.

Electrode	Mass median aerodynamic diameter MMAD (μm)	Geometrical standard deviation (GSD)
N	0.3787	2.12
C1	0.3783	1.51
C2	0.3774	2.32
C3	0.3697	1.71
C4	0.3647	2.32
C5	0.3599	1.98

3.3. *Fume morphology*

The morphology of fume particulates, collected during various stages of the cascade impactor, were characterized using SEM imaging. In all the tested fume samples, three distinct types of particle morphology viz. spherical, irregular and agglomerated were observed at each impaction stage as shown in Fig. 7. Agglomerated particles were found to be prevalent at all stages. Cooling mechanism from the vapour state caused small welding fume particles to coalesce into large spherical agglomerated particles. Isolated spherical particles were also observed, but their proportion was found to be relatively less. Irregular-shaped particles were the least prevalent among three identified morphologies.

Morphological samples collected from the conventional electrode and electrode C5 (which produced the lowest quantity of fumes) were compared and their SEM images taken at various impactor stages are shown in Fig. 8. A notable shift in particle concentration can be observed in the SEM images during the different impactor stages. Fig. 8(a–d) reveals that, polydispersed particles with distinct agglomeration sizes were noted in the conventional electrode's fumes. Particle polydispersity has a vital role in lung deposition. A higher concentration of different size particles may hinder normal lung functioning. It is apparent that, for the conventional electrode, impactor stage A comprised more agglomerated particles with a seemingly higher particle size. Larger agglomerates increased mass concentration and increased their deposition in the lungs including the alveolar region [33–34]. The agglomeration of fume particles would have contributed to the higher mass concentration in the conventional electrode.

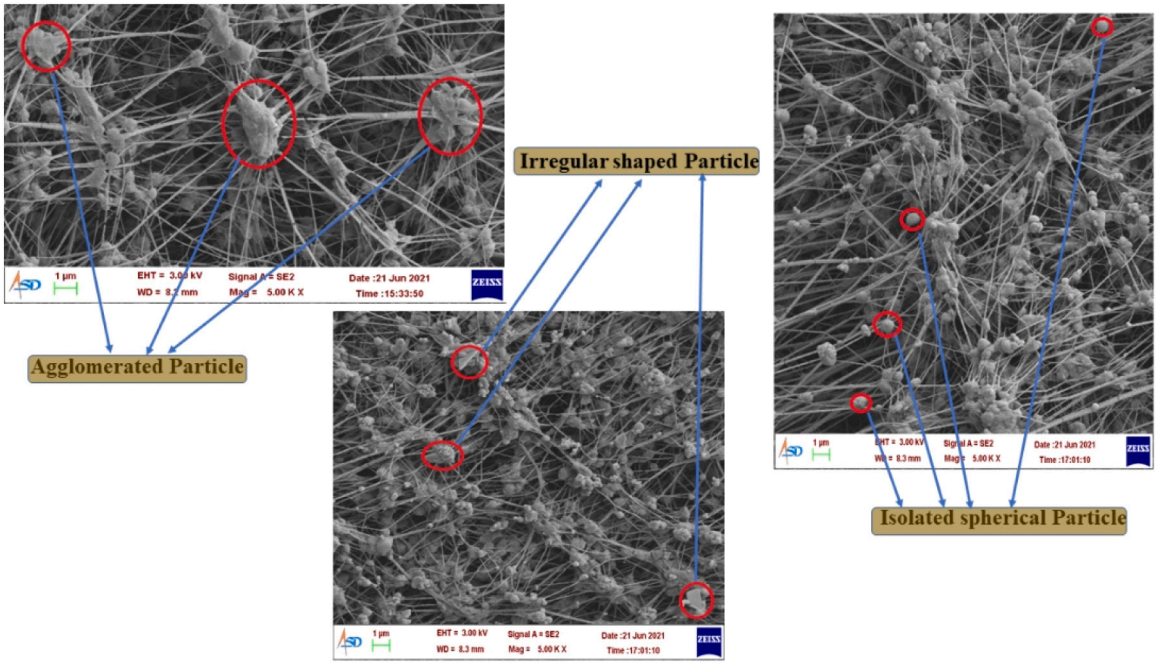

Fig. 7. Fume particulate morphology.

Fig. 8(e–h) shows the SEM images of fume samples from the experimental electrode C5. A discernible variation in concentration of various fume particles can be noted at each impactor stage compared to the conventional electrode. Compared to the conventional electrode, a monodispersed suspension of particles of nearly the same size was observed in the experimental samples. Micro or monodispersed particles are easy for the macrophages to phagocytize but agglomerated large particles are harder to remove from the lungs. Particles that were not phagocytized were retained in the interstitium and in epithelial cells. In experimental electrodes, reduction in the concentration of agglomerates was noted, which related to the lower mass concentration observed in Fig. 5. At lower impaction stages, the monodispersed particles, are more concentrated than those in the conventional electrode. This might be the reason for the lower MMAD values for C5 presented in Table 3. Morphological analysis concludes that, nano-$CaTiO_3$ particle added to the welding flux have a significant influence on particle shape formation.

The morphological shape of particles was quantified by using shape descriptors such as circularity, convexity and elongation as shown in Fig. 9. Circularity is described as particle roundness; convexity as parameter describing the surface roughness with, elongation being the measure of difference between the minor and major axis. It was evident from the figure that conventional electrode fumes indicated lower circularity, convexity and higher elongation. In contrast, experimental electrode C5 emitted fume particles with higher circularity, convexity and low elongation. The high circularity and convexity indicate that most particles were monodispersed and of nearly the same size. In conventional fumes, most particles were irregular in shape with a polydispersed structure.

3.4. Particle size distribution

The CMD value represents the size segregation of fumes at each impactor stage based on the count of particulates collected. Table 4 shows the count median diameter estimated from the SEM images and the geometric standard deviation of fume particles at each impactor stage. The CMD value was found to decrease with an increase in the amount of nano-$CaTiO_3$ in the flux.

For 100 % addition of nano-$CaTiO_3$ (electrode C5), the CMD at the impaction stage A reduced by 1.12 % compared to the conventional electrode, while at impaction stages B, C and D the reduction was 4.14 %, 0.85 % and 1.8 % respectively. A reduction in CMD was invariably noticed, at all impactor stages as the nano-$CaTiO_3$ concentration increased. Further, it could be observed that the size of ultrafine particles collected at the impactor stage D of the conventional electrode was 495 nm. Whereas, the mean particle diameters were 493 nm (0.40 % reduction), 491 nm (0.80 % reduction), 489 nm (1.21 % reduction), 488 nm (1.41 % reduction) and 486 nm (1.81 % reduction), respectively for the experimental electrodes C1, C2, C3, C4 and C5. Reduction in particle diameter could be due to the formation of more monodispersed fume particulate. This shows that the addition of nano-$CaTiO_3$ particles to the welding flux indisputably influenced particle size formation in the fume. In the present work, size reduction was less than 5 % which was insignificant compared to the appreciable reduction in fume by 50 %.

3.5. Viability of the newly developed electrode on reduction of health issues

Welding fume contains a complex mixture of metallic oxides, silicates and fluorides which are potentially hazardous and poses serious threats to the operating personnel. There have been reports that the workers are badly affected due to the toxic effect of welding fumes. Many researchers have reported the hazardous effects of particles size, shape and biological activity of welding fumes on human health as well on the environment [35–37]. Though several control methods have been proposed for fume reduction, only few were suitable to a SMAW process. The most promising control strategy is the reduction of fumes at the source by suitable modifications of the consumables.

In the present study nano-sized $CaTiO_3$ was used as an arc stabilizer in the welding flux of a SMAW process, with the primary objective of reducing the fume emissions at the source. The concentration of metallic oxides in fumes from the newly developed electrodes (nano -$CaTiO_3$ coated) were found to reduce due to the increased dragging effect of the weld pool [38]. The reduction of hazardous constituents in the weld atmosphere, in turn reduces the risk of the operator due to occupational exposure to welding fume.

The results of the investigation showed that for 100 % addition of nano- $CaTiO_3$, in the flux, a reduction of 98.75 % in particulate matter

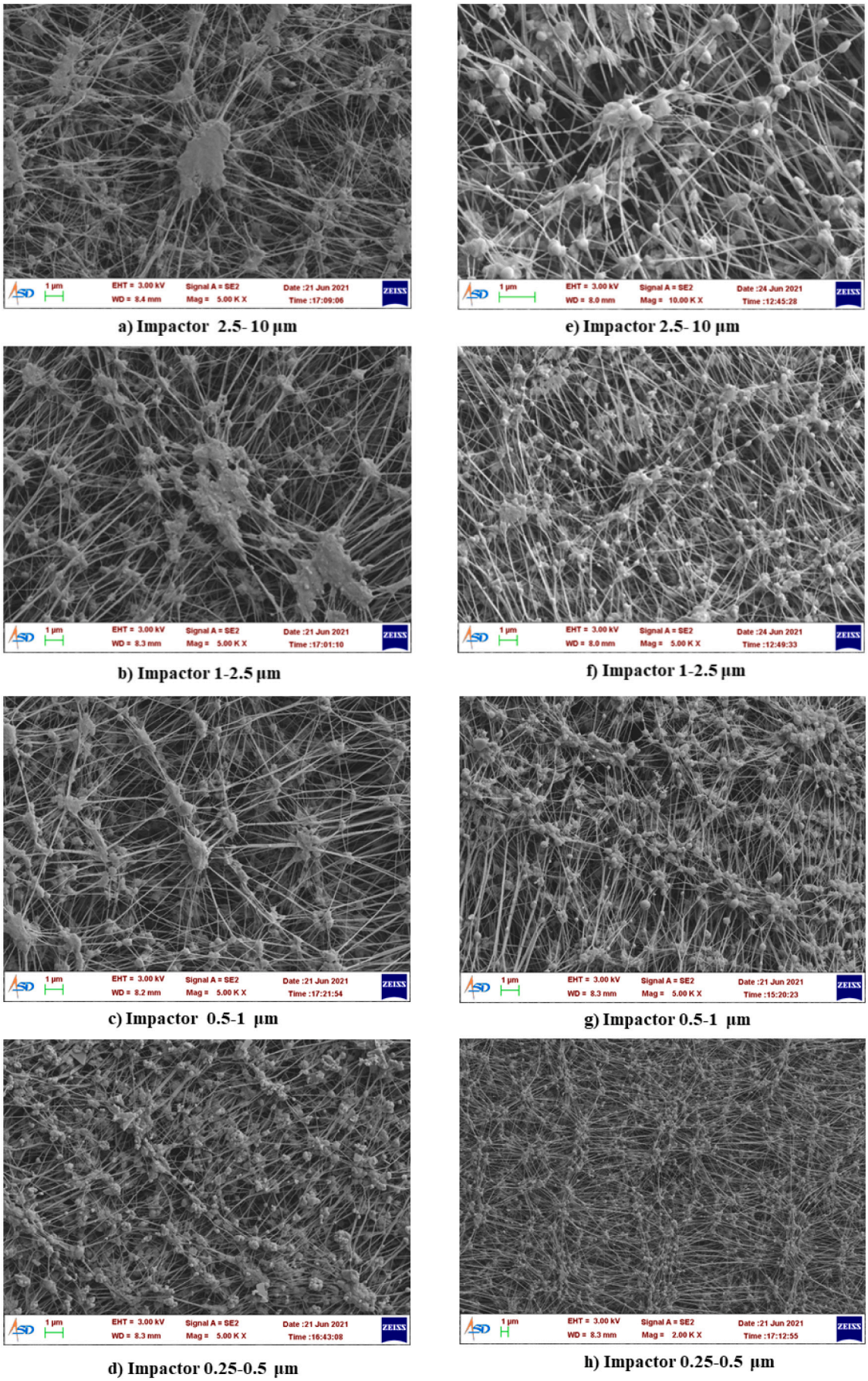

Fig. 8. (a–d) SEM of a conventional electrode fume particles, (e–h) SEM of C5 experimental electrode fume particles collected at various stages of cascade impactor.

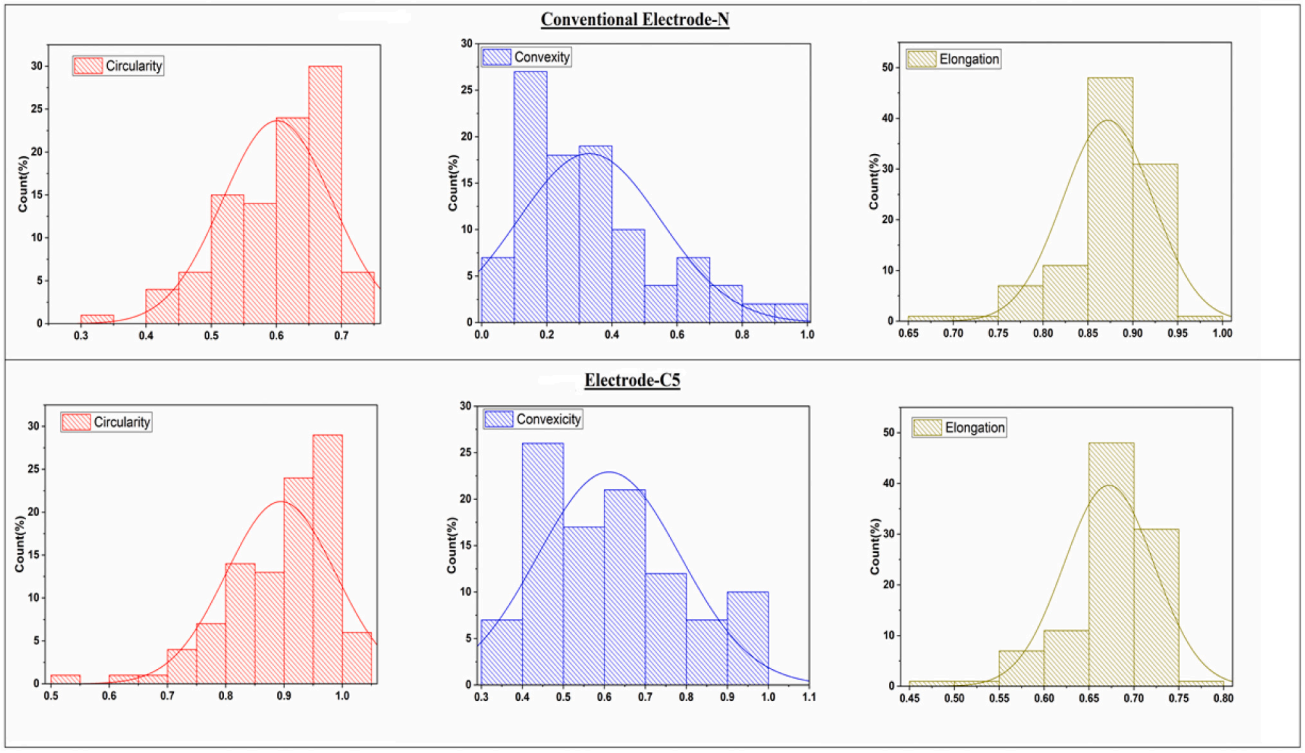

Fig. 9. Distribution of particle shape descriptors.

Table 4
Particle count median diameter and geometric standard deviation.

Electrode	Impactor stage	Count median diameter (CMD)	Geometric standard deviation (σ_g)
N	A	6.21 μm	1.2
	B	2.41 μm	1.4
	C	0.931 μm	1.1
	D	0.495 μm	1
C1	A	6.19 μm	1.5
	B	2.39 μm	1.3
	C	0.929 μm	1.2
	D	0.493 μm	1.1
C2	A	6.18 μm	1.4
	B	2.37 μm	1.3
	C	0.928 μm	1.2
	D	0.491 μm	1.1
C3	A	6.17 μm	1.6
	B	2.36 μm	1.5
	C	0.927 μm	1.3
	D	0.489 μm	1.1
C4	A	6.15 μm	1.3
	B	2.34 μm	1.2
	C	0.924 μm	1.3
	D	0.488 μm	1.1
C5	A	6.14 μm	1.3
	B	2.31 μm	1.2
	C	0.923 μm	1.3
	D	0.486 μm	1.1

size above 2.5 μm, 96 % in particulate matter size 1–2.5 μm, 68.1 % in particulate matter size 0.5–1 μm and 48.8 % in particulate matter size 0.25–0.5 μm were observed from the experimental electrodes indicating an effective reduction in the inhalable and respirable fraction of fume. Which indicating that in all the size ranges comparing with the conventional one experimental electrode effectively reduces the particle mass concentration.

Further, it was observed that, the addition of nano-$CaTiO_3$ to the welding flux caused, a nominal reduction in the Mass Median Aerodynamic Diameter (MMAD) value. Even though the reduction in MMAD was not preferable, when compared to the reduction of fumes by up to 50 %, a minimal reduction of (less than 5 %) MMAD will not be of serious concern. The morphological analysis of the conventional electrode indicated the presence of a higher amount of polydispersed particles in the welding fume. In the experimental electrode's fumes, instead of polydispersed particles, monodispersed particles were prevalent which in turn could reduce the inhalation risk [33].

Overall, the experimental results indicated that the novel coated electrodes presented in this paper could reduce both acute and chronic health risks associated with welding fumes. An artistic impression showing the hazard reduction is given in Fig. 10.

4. Conclusion

This study investigated the effect of nano-$CaTiO_3$ on the mass concentration, morphology and size of the welding fume particulates. The major findings of the study are given below.

- Nano-$CaTiO_3$ have a substantial influence on the rate of fume formation and breathing zone concentration. Electrodes assaying 100 % nano-$CaTiO_3$ (electrode C5) ensured a 48.85 % reduction in fume formation rate and 54.04 % reduction breathing zone concentration compared to the conventional electrode.
- Weld spatter was visualised with an infrared camera. Compared to the conventional electrode, the experimental electrodes had a lower spatter density. This indicated that nano-$CaTiO_3$ was useful in reducing welding spatter.
- The mass concentration on different size ranges of fume particles was obtained using a cascade impactor. A reduction of 98.75 % in particulate matter size 2.5, 96 % in particulate matter size 1, 68.1 % in particulate matter size 0.5 and 48.8 % in particulate matter size 0.25 were observed in the experimental electrode when the whole micro sized $CaTiO_3$ was replaced with its nano sized counterpart.
- The mass median aerodynamic diameter and corresponding standard deviations were found from the cumulative probability cure. A minor

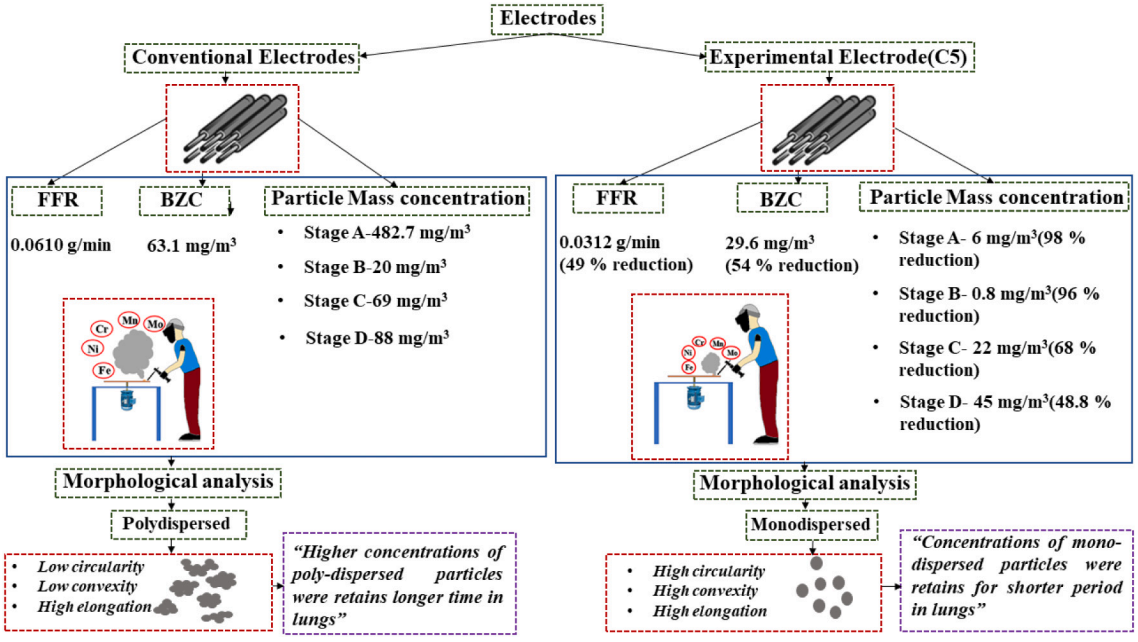

Fig. 10. Artistic illustration on the comparison of conventional and experimental electrode health effects.

reduction in mass median aerodynamic diameter value was observed with the addition of nano- $CaTiO_3$ addition. Though a reduction in mass median aerodynamic diameter was not preferable, compared to the reduction of fumes by up to 50 %, a minimal reduction of 4.96 % in mass median aerodynamic diameter was not of serious concern.

- The morphological analysis revealed the presence of agglomerated, spherical and irregular fume particles at all impactor stages. The morphological analysis of conventional electrode indicated the presence of higher amounts of polydisperse particles in the welding fume. In the C5 electrode's fumes, monodispersed particles instead of polydisperse particles, were prevalent which in turn reduced inhalation risk.
- The count median diameter and standard deviation were calculated by post processing the SEM images to measure particle size collected on each impactor plate. The count median diameter was found to decrease with an increase in nano- $CaTiO_3$ in the flux. Maximum particle size reduction obtained was below 5 % in comparison to the appreciable reduction in fume formation rate (48.8 %) and breathing zone concentration (54.04 %).

CRediT authorship contribution statement

Mr. Rahul M: Conceptualization, Methodology, Investigation, Writing - original draft.

Dr. S.P. Sivapirakasam: Formal analysis, Supervision, Resources, Writing - review & editing.

Dr. Sreejith Mohan: Methodology, Validation, Formal analysis, Investigation.

Dr. Vishnu B. R: Formal analysis, Investigation.

Dr. João Gomes: Review & editing.

Declaration of competing interest

The authors declare that they have no known competing financial interests or personal relationships that could influence the work reported in this paper.

Acknowledgments

The authors are grateful to the Director, National Institute of Technology (NIT), Tiruchirappalli for her continual encouragement and support for this work.

References

[1] Antonini JM, Lewis AB, Roberts JR, Whaley DA. Pulmonary effects of welding fumes: review of worker and experimental animal studies. Am J Ind Med 2003;43:350–60.
[2] Vishnyakov VI, Kiro SA, Ennan AA. Reducing of UV radiation intensity, ozone concentration and fume formation in gas metal arc welding. Aerosol Sci Eng 2020;4:192–9.
[3] McMillan GH, Pethybridge RJ. The health of welders in naval dockyards: proportional mortality study of welders and two control groups. Occup Med 1983;33(2):75–84.
[4] Xing YF, Xu YH, Shi MH, Lian YX. The impact of PM 2.5 on the human respiratory system. J Thorac Dis 2016;8(1):69.
[5] Mendez PF, Barnes N, Bell K, Borle SD, Gajapathi SS, Guest SD, Wood G. Welding processes for wear resistant overlays. J Manuf Process 2014;16(1):4–25.
[6] Voitkevich V. Welding fumes: formation, properties, and biological effects. Woodhead Publishing Limited; 1995.
[7] Hoffman DJ, Reynolds RM, Hardy DB. Developmental origins of health and disease: current knowledge and potential mechanisms. Nutr Rev 2017;75:951–70.
[8] Popović O, Prokić-Cvetković R, Burzić M, Lukić U, Beljić B. Fume and gas emission during arc welding: hazards and recommendation. Renew Sustain Energy Rev 2014;37:509–16.
[9] Sivapirakasam SP, Mohan S, Kumar MS, Surianarayanan M. Welding fume reduction by nano-alumina coating on electrodes–towards green welding process. J Clean Prod 2015;108:131–44.
[10] Mohan S, Sivapirakasam SP, Kumar MS, Surianarayanan M. Welding fumes reduction by coating of nano-TiO2 on electrodes. J Mater Process Technol 2015;219:237–47.
[11] Vishnu BR, Sivapirakasam SP, Satpathy KK, Albert SK, Chakraborty G. Influence of nano-sized flux materials in the reduction of the Cr (VI) in the stainless-steel welding fumes. J Manuf Process 2018;34:713–20.
[12] Jenkins NT, Pierce WMG, Eagar TW. Particle size distribution of gas metal and flux cored arc welding fumes. Weld J 2005;84:156–63.
[13] Sowards JW, Lippold JC, Dickinson DW, Ramirez AJ. Characterization of welding fume from SMAW electrodes-part I. Weld J 2008;87:106. New York.
[14] Adachi K, Chung SH, Buseck PR. Shapes of soot aerosol particles and implications for their effects on climate. J Geophys Res Atmos 2010;115:15.
[15] Ghio AJ, Devlin RB. Inflammatory lung injury after bronchial instillation of air pollution particles. Am J Respir Crit Care Med 2001;164:704–8.
[16] Hinds WC. Aerosol technology: properties, behavior, and measurement of airborne particles. John Wiley & Sons; 1999.
[17] ISO Standard: ISO 15011-1:2009: Health and Safety in Welding and Allied Processes – Laboratory Method for Sampling Fume and Gases Generated by Arc Welding – Part 1: Determination of Emission Rate and Sampling for Analysis of Particulate Fume.
[18] ISO 10882-1. Health and safety in welding and allied processes e sampling of airborne particles and gases in the operator's breathing zone e part 1: sampling of airborne particles. 2011.

[19] Lin CC, Chen MR, Chang SL, Liao WH, Chen HL. Characterization of ambient particles size in workplace of manufacturing physical fitness equipments. Ind Health 2015;53(1):78–84.
[20] Isaxon C, Pagels J, Gudmundsson A, Asbach C, John AC, Kuhlbusch TAJ, Bohgard M. Characteristics of welding fume aerosol investigated in three Swedish workshops. In: Journal of Physics: Conference Series. 151(1). IOP Publishing; 2009.
[21] Takahashi J, Nakashima H, Fujii N. Fume particle size distribution and fume generation rate during arc welding of cast iron. Ind Health 2020;2019:0161.
[22] Karlsen JT, Farrants G, Torgrimsen T, Reith.. A chemical composition and morphology of welding fume particles and grinding dusts. Am Ind Hyg Assoc J 1992;53(5):290–7.
[23] Güney B. Microstructure analysis of welding fume of low and medium carbon steels. Rev Metal 2021;57:187.
[24] Floros N. Welding fume main compounds and structure. Weld World 2018;62(2): 311–6.
[25] Zimmer AT, Biswas P. Characterization of the aerosols resulting from arc welding processes. J Aerosol Sci 2001;32:993–1008.
[26] Hedberg YS, Wei Z, McCarrick S, Romanovski V, Theodore J, Westin EM, Wallinder IO. Welding fume nanoparticles from solid and flux-cored wires: solubility, toxicity, and role of fluorides. J Hazard Mater 2021;413:125273.
[27] Acharya U, Roy BS, Saha SC. Torque and force perspectives on particle size and its effect on mechanical property of friction stir welded AA6092/17.5 SiCp-T6 composite joints. J Manuf Process 2019;38:113–21.
[28] Trinh NQ, Tashiro S, Tanaka K, Suga T, Kakizaki T, Yamazaki K, Tanaka M. Effects of alkaline elements on the metal transfer behavior in metal cored arc welding. J Manuf Process 2021;68:1448–57.
[29] Chen B, Han F, Huang Y, Lu K, Liu Y, Li L. Influence of nanoscale marble (calcium carbonate CaCO3) on properties of D600R surfacing electrode. Weld J 2009;88: 99s–103s. Research Supplement.
[30] Jia C, Zhang Y, Wu J, Xing C, Zhao B, Chuansong W. Comprehensive analysis of spatter loss in wet FCAW considering interactions of bubbles, droplets and arc–part 2: visualization & mechanisms. J Manuf Process 2019;40:105–12.
[31] Berlinger B, Náray M, Záray G. Distribution of metals between inhalable and respirable fractions of welding fumes generated in gas metal arc welding. Sci Technol Weld Join 2008;13:721–5.
[32] Yang SY, Lin JM, Young LH, Chang CW. Mass-size distribution and concentration of metals from personal exposure to arc welding fume in pipeline construction: a case report. Ind Health 2018;2017:0197.
[33] Braakhuis HM, Park MV, Gosens IDe, Jong WH, Cassee FR. Physicochemical characteristics of nanomaterials that affect pulmonary inflammation. Part Fibre Toxicol 2014;11:1–25.
[34] Hautanen J, Kilpeläinen M, Kauppinen EI, Lehtinen K, Jokiniemi J. Electrical agglomeration of aerosol particles in an alternating electric field. Aerosol Sci Technol 1995;22:181–9.
[35] Beach JR, Dennis JH, Avery AJ, Bromly CL, Ward RJ, Walters EH, Hendrick DJ. An epidemiologic investigation of asthma in welders. Am J Respir Crit Care Med 1996; 154(5):1394–400.
[36] Han BC, Liu I, Chuang HC, Pan CH, Chuang KJ. Effect of welding fume on heart rate variability among workers with respirators in a shipyard. Sci Rep 2016;6(1): 1–6.
[37] Zadafiya K, Shah P, Shokrani A, Khanna N. Recent advancements in nano-lubrication strategies for machining processes considering their health and environmental impacts. J Manuf Process 2021;2021(68):481–511.
[38] Pal TK, Maity UK. Effect of nano size TiO2 particles on mechanical properties of AWS E 11018M type electrode. Mater Sci Applic 2011;2(09):1285.